Supplementary Material: Physical model for the geometry of actin-based cellular protrusions

G. Orly, M. Naoz and and N. S. Gov*
Department of Chemical Physics, The Weizmann Institute of Science, P.O. Box 26, Rehovot, Israel 76100

PACS numbers:

POLYMERIZATION RATE DECREASING WITH HEIGHT

When the actin polymerization at the tip is limited by the supply of G-actin that is transported by diffusion from the cytoplasm (protrusion base), we get that

$$A = A_0 \frac{1}{1 + h/h_D} \tag{S1}$$

where A_0 is the polymerization rate given the concentration of G-monomers at the protrusion base, $h_D = D * k_{on}/\delta$, where D is the diffusion coefficient of the G-actin along the protrusion, k_{on} is the rate of incorporation per G-actin at the tip and δ is the size of a monomer.

Under these conditions, a steady-state height of a cylindrical protrusion is possible even for a constant restoring force of a tubular membrane (Eq.4). The steady-state height, instead of Eq.(10) is now given by (assuming we are dominated by tension in Eq.4)

$$h_{st} = \frac{\sqrt{2}\sqrt{A_0^2\beta\gamma_c h_c^2 h_d^2 R\sigma^2\left(\sqrt{4h_c^2\sigma^2 + \beta^2\gamma_c^2 R^2} + \beta\gamma_c R\right)} - 2\beta h_c^2 h_d \sigma^2}{2\beta h_c^2 \sigma^2} \tag{S2}$$

For $R \ll 2h_c\sigma/(\beta\gamma_c)$ the height increases as $\sqrt{R}$, and linearly with R for large R.

CALCULATION OF THE POLYMERIZATION RATE $A(h)$ FOR THE CASE OF A TIP-TRANSPORTED PROMOTER

Let us demonstrate an example of an explicit calculation of $A(h)$ for the case of a single type of promoter of actin polymerization that is carried to the tip by a myosin motor. We consider that the cargo protein plus its carrying motor form a single complex (for simplicity), which can either move processively to the tip at the velocity $v_m = v_w - v_a$ (where v_w is the processive velocity of the motor on the actin filaments), or detach from the actin and diffuse freely in the protrusion with diffusion coefficient D. This is identical to the case treated in [1] and the equations are the same as Eqs.16,17

$$\dot{\rho_f} = D\nabla_z^2\rho_f + k_{off}\rho_b - k_{on}\rho_f \tag{S3}$$

$$\dot{\rho_b} = v_m\nabla_z\rho_b - k_{off}\rho_b + k_{on}\rho_f \tag{S4}$$

The resulting distribution of the free and actin-bound complexes along the length of the protrusion are given by [1]

$$\begin{aligned}\rho_f(z) &= \frac{1}{2\sqrt{D}\left(Dk_{off}^2+4k_{on}v_m^2\right)}\Big[\exp\left(\frac{x\left(\sqrt{D}k_{off}-\sqrt{Dk_{off}^2+4k_{on}v_m^2}\right)}{2\sqrt{D}v_m}\right)\\ &\left(D^{3/2}k_{off}^2\rho_{f,0}\left(e^{\frac{x\sqrt{Dk_{off}^2+4k_{on}v_m^2}}{\sqrt{D}v_m}}+1\right)\right.\\ &-Dk_{off}\rho_{f,0}\sqrt{Dk_{off}^2+4k_{on}v_m^2}\left(e^{\frac{x\sqrt{Dk_{off}^2+4k_{on}v_m^2}}{\sqrt{D}v_m}}-1\right)\\ &+4\sqrt{D}k_{on}\rho_{f,0}v_m^2\left(e^{\frac{x\sqrt{Dk_{off}^2+4k_{on}v_m^2}}{\sqrt{D}v_m}}+1\right)\\ &\left.-2\rho_{b,0}v_m^2\sqrt{Dk_{off}^2+4k_{on}v_m^2}\left(e^{\frac{x\sqrt{Dk_{off}^2+4k_{on}v_m^2}}{\sqrt{D}v_m}}-1\right)2\sqrt{D}\left(Dk_{off}^2+4k_{on}v_m^2\right)\right]\end{aligned} \tag{S5}$$

$$\begin{aligned}\rho_b(z) &= \frac{1}{2\left(Dk_{off}^2+4k_{on}v_m^2\right)}\Big[\exp\left(\frac{x\left(\sqrt{D}k_{off}-\sqrt{Dk_{off}^2+4k_{on}v_m^2}\right)}{2\sqrt{D}v_m}\right)\\ &\left(\sqrt{D}(k_{off}\rho_{b,0}-2k_{on}\rho_{f,0})\sqrt{Dk_{off}^2+4k_{on}v_m^2}\left(e^{\frac{x\sqrt{Dk_{off}^2+4k_{on}v_m^2}}{\sqrt{D}v_m}}-1\right)\right.\\ &\left.+Dk_{off}^2\rho_{b,0}\left(e^{\frac{x\sqrt{Dk_{off}^2+4k_{on}v_m^2}}{\sqrt{D}v_m}}+1\right)+4k_{on}\rho_{b,0}v_m^2\left(e^{\frac{x\sqrt{Dk_{off}^2+4k_{on}v_m^2}}{\sqrt{D}v_m}}+1\right)\right)\Big]\end{aligned} \tag{S6}$$

where k_{on}, k_{off} are the on/off rates from the actin-bound to free states, and $\rho_{f,0}, \rho_{b,0}$ are the concentrations of the free and actin-bound complexes at the protrusion base (cytoplasm). We plot this distribution in Fig.S1a.

Using the concentration of free promoter at the tip $\rho_f(h) = C_p(h)$ from Eq.S5 in Eq.8 (assuming that the free promoter is available to interact at the tip and affect the polymerization rate), we get $A(h)$

$$A(h) = \frac{A_f + A_p K_p C_p(h)}{1 + K_p C_p(h)} \tag{S7}$$

In Fig.S1b we plot the result of Eq.S7 for various parameters.

We can get an estimate of the height h at which $A(h)$ has an inflection point, by noting that usually $v_w \gg v_a$ and solving for the height at which $1 = K_p C_p(h)$. We get

$$\begin{aligned}h_{inflection} &\simeq \frac{2\sqrt{D}v_m}{\sqrt{D}k_{off}-\sqrt{Dk_{off}^2+4k_{on}v_m^2}}\\ &\log\left(\frac{2\sqrt{D}\left(Dk_{off}^2+4k_{on}v_m^2\right)}{K_p\left(D^{3/2}k_{off}^2\rho_{f,0}+Dk_{off}\rho_{f,0}\sqrt{Dk_{off}^2+4k_{on}v_m^2}+2\rho_{b,0}v_m^2\sqrt{Dk_{off}^2+4k_{on}v_m^2}+4\sqrt{D}k_{on}\rho_{f,0}v_m^2\right)}\right)\end{aligned} \tag{S8}$$

This estimate is denoted by the dashed vertical lines in Fig.S1b, and gives a very good estimate of the inflection point. We find that the inflection point moves to larger heights when the motor velocity decreases (green line in Fig.S1b) or the affinity of the promoter decreases (black line in Fig.S1b).

GROWTH DYNAMICS

Constant tip-complex radius

We begin this section by studying the height dynamics of the protrusion, for the case of a constant radius of the tip complex. The height dynamics of a cylindrical protrusion is presented in (Eq.7) and the numerical solution is

plotted in Fig.S2 for four representative cases: constant polymerization rate with no initial tail (Fig.S2a), constant polymerization rate with a long initial tail (Fig.S2b), polymerization rate that increases with height (Fig.S2c) and the collapse following the termination of the polymerization (Fig.S2d).

For the simple case of a cylindrical protrusion where there is a single steady-state solution and there is no extrema in the total protrusive force ($F_{tot} \equiv F_a - F_{md} - F_{ma}$, Eqs.1,3-6), and taking $\mu \sim 0$, we find that the dominant restoring force is due to $F_{ma} \propto h$. Taking a constant polymerization rate A, we can simplify (Eq.7) in the form

$$\gamma_c(A - \dot{h})S_c = 2\alpha R_{tip} h. \tag{S9}$$

If $\dot{h}$ is small, such that the rootlet achieves a steady-state conical shape (Eq.9), we can write

$$\gamma_c R_{base}^2 \sqrt{1 + \left(\frac{A - \dot{h}}{\beta}\right)^2}\,(A - \dot{h}) = 2\alpha R_{tip} h. \tag{S10}$$

This equation can be solved analytically in four regimes:

When the protrusion starts growing from a very short initial tail the growth rate can be approximated by: $\dot{h} = A$. As the protrusion elongates further the growth rate decays exponentially to zero ($A \gg \dot{h}$) with time scale of

$$\tau_h = \frac{h_{st}}{A}. \tag{S11}$$

where h_{st} is the steady-state height (Eq.10).

The analytical solutions in both these limits have an initial slope of $\dot{h} = A$ which is the maximal possible growth rate (cases 1,2 in Table I). The exact numerical solution has a smaller slope since the protrusion does not just elongate at the initial stages but also forms the rootlet needed for support (Fig.S2a).

A different dynamics arises when the protrusion has a long initial rootlet, before it starts protruding from the cell, as is found experimentally in some cases [3]. We now find that the height makes an over-shoot above the steady-state height, and decays towards the steady-state value as the initial rootlet is severed (Fig.S2b). A large initial rootlet allows the protrusion to grow at a fast rate (reaching the maximal rate of $\dot{h} = A$) and therefore reach a significant height sooner. In a case where more than a single steady-state height exists, this may allow reaching higher solutions.

When $F_{tot}(h)$ has extrema, we can acquire the growth dynamics that leads to the higher branch (or branches) of steady-state solutions while the growth rate is still affected by the proximity of an additional solution (Fig.S2c). This situation can occur for example when the restoring force is simply linear with h, but the polymerization rate increases with h and has an inflexion point $A''(h) = 0$, as shown. Other possible combinations of restoring and protrusive forces can also give rise to this behavior.

To conclude, while there is polymerization we find that the height is a monotonously increasing function of time, unless there is a large initial rootlet that gives rise to an over-shoot behavior.

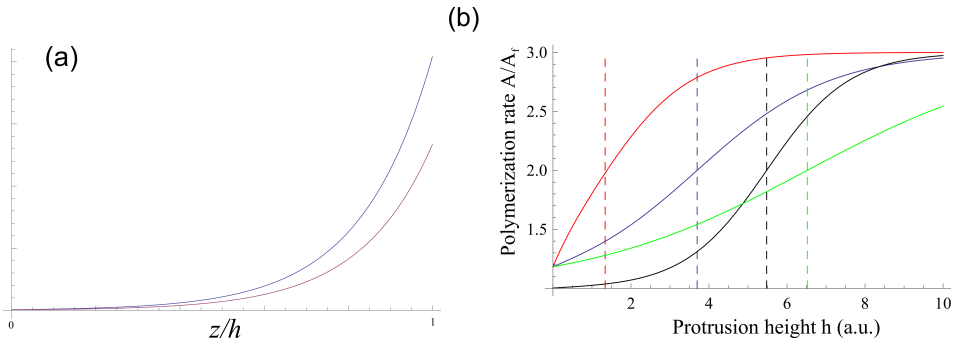

FIG. S1: (a) Concentration profiles of the myosin-plus-cargo complex along the protrusion height z, for a tip-directed transport (Eqs.S5,S6 [1]). Blue line is for the free component ρ_f, and purple for the actin-bound component ρ_b, (using the parameters (arbitrary units): $v_a = 0.1, v_w = 1, k_{on} = 1, k_{off} = 1, D = 1, \rho_{f,0} = \rho_{b,0} = 0.1$). (b) Calculation of the polymerization rate $A(h)$ as a function of the protrusion height, using Eq.S7 (Eq.8) and the distribution of the free component from Eq.S5, using $K_p = 1, A_f = 1, A_p = 3$. Blue is for the same parameters as in (a), while red is for $v_w = 5$, black is for $v_w = 10, K_p = 0.01$, and green for $v_w = 0.5, K_p = 1$. The vertical dashed lines give the estimated location of the inflection point given by $h_{inflection}$ (Eq.S8).

When the polymerization is terminated the protrusion retracts with an initial rate that is approximately constant. Only when the protrusion is small one observes slower than linear decay until the protrusion finally disappears (Fig.S2d). For the parameters taken in this example we see a good fit of the numerical solution to the case where $\dot{h} \gg \beta$ (case 3 in Table I).

Dynamics of the height and the tip complex radius combined

The dynamical width regulation mechanism for a cylindrical protrusion (Eq.21) can be written in the limit of $R_{tip} \ll \sqrt{D_{tip}/k_{tip}}$ (which as discussed below is probably the biologically relevant regime) as

$$\dot{R_{tip}} = \frac{\chi}{R_{tip}} - \eta \tag{S12}$$

where $\chi = 2J_{eff}k_{on}^{nuc}c_{nuc}/k_{tip}$ and $J_{eff} = v_m u_0 \frac{R_{base}}{R_{tip}} \frac{k_{on}^u}{k_{off}^u}$ (R_{base}/R_{tip} is a constant in a cylindrical protrusion). The solution of this equation is in the form of a Lambert W-function, which is monotonously increasing with time up to the steady-state value $R_{tip}^{st} = \chi/\eta$. The time-scale for this growth is given by

$$\tau_R = \frac{R_{tip}^{st}}{\eta}. \tag{S13}$$

In Fig.S3 we plot the calculated growth dynamics of both the tip-complex radius and protrusion height for $O(\tau_h) = O(\tau_R)$. Note that in the case where $\tau_h \ll \tau_R$ the initial radius must be large enough so that the protrusion will not disappear before reaching a sufficient length.

STEADY-STATE CONICAL PROTRUSIONS

In the case of a constant severing rate β along the protrusion the result is a conical shaped protrusion as presented in Fig.S4

We begin by analyzing the steady-state height for this geometry, for a fixed radius of the tip complex R_{tip}. The protrusive force of the actin treadmilling is $F_a = \gamma_c S_c(h) A(h)$ (Eq.1, at steady-state $\dot{h} = 0$) and the rootlet area S_c (Eq.9) is now given by

$$S_c(h) = \pi[R_{tip} - (\beta/A)h]^2\sqrt{1 + (A/\beta)^2} \tag{S14}$$

TABLE I: Analytical expressions for the growth dynamics of different scenarios.

	case	Equation	result
1	$A \gg \dot{h}$	$\dot{h} = A - \frac{2\alpha R_{tip} h}{\gamma_c R_{base}^2 \sqrt{1+(A/\beta)^2}}$	$h(t) = h_{st}\left(1 - e^{-t/\tau_h}\right) \quad \tau_h = \frac{h_{st}}{A}$
	h_{st} is the steady-state height (Eq.10).		
2	$A \simeq \dot{h}$	$\gamma_c(A - \dot{h})S_c(0) = 2\alpha R_{tip} h$	$h(t) = A\omega(1 - e^{-t/\omega}), \quad \omega = \frac{\gamma_c S_c(0)}{2\alpha R_{tip}}$
	$S_c(0)$ is the initial rootlet. This case corresponds to the initial growth.		
3	$A = 0$, $\dot{h} \gg \beta$	$(\dot{h})^2 = \frac{2\alpha\beta R_{tip}}{\gamma_c R_{b2}} h$	$h(t) = \frac{\left(\sqrt{2\alpha\beta R_{tip}}t - 2R_{base}\sqrt{\gamma_c h_{st}}\right)^2}{4\gamma_c R_{base}^2}$
	The initial retraction stage following the termination of the polymerization.		
4	$A = 0$, $\dot{h} \ll \beta$	$\dot{h} = -\frac{2\alpha R_{tip}}{\gamma_c R_{b2}} h$	$h(t) = h_{st} e^{-t/\tilde{\omega}}, \quad \tilde{\omega} = \frac{\gamma_c R_{base}^2}{2\alpha R_{tip}}$
	The final retraction stage following the termination of the polymerization.		

where h can range between zero and the maximal height $h_{max} = R_{tip}A/\beta$, and is determined by the force balance (Eq.7). The protrusive force is monotonously decreasing with height when

$$A'(h) < \frac{\beta}{\Omega R_{tip} + (1-\Omega)(\beta/A)h}$$

where $\Omega \equiv [1+2(A/\beta)^2]/[2+2(A/\beta)^2]$, and otherwise increasing with the height, as shown in Fig.S5.

Therefore if the polymerization rate depends on the height, as was found for the case of stereocilia [2], it is possible to have an extremum (or even several extrema) in $F_a(h)$, depending on the nature of $A(h)$. As we shall see this allows the option of multiple steady-state heights.

The restoring forces applied by the membrane and the myosin motors are

$$F_{md} = 2\pi\kappa\frac{A}{\beta}\frac{1}{\sqrt{1+\left(\frac{\beta}{A}\right)^2}L_{root}} + 2\pi\sigma\frac{\beta}{A}\sqrt{1+\left(\frac{\beta}{A}\right)^2}L_{root} \tag{S15}$$

$$F_{ma} = \pi\alpha\frac{\beta}{A}\sqrt{1+\left(\frac{\beta}{A}\right)^2}\left(h^2+2hL_{root}\right) \tag{S16}$$

The results are plotted in Fig.S6 for the case of a constant polymerization rate, and for an increasing $A(h)$ as given in the inset. For a constant polymerization rate we find that there is only a single stable steady-state solution and the height grows linearly with the tip-complex radius. For the case of an increasing (steeply enough) $A(h)$ there can be additional stable steady-states heights. In general, for all realistic types of the restoring force the maximal number of stable steady-state solution is $[N/2]+1$ where N is the number of extrema of $F_a(h)$.

Note that the sharp increase in the membrane restoring force at large heights arises from the very narrow rootlet of the conical protrusion in this limit.

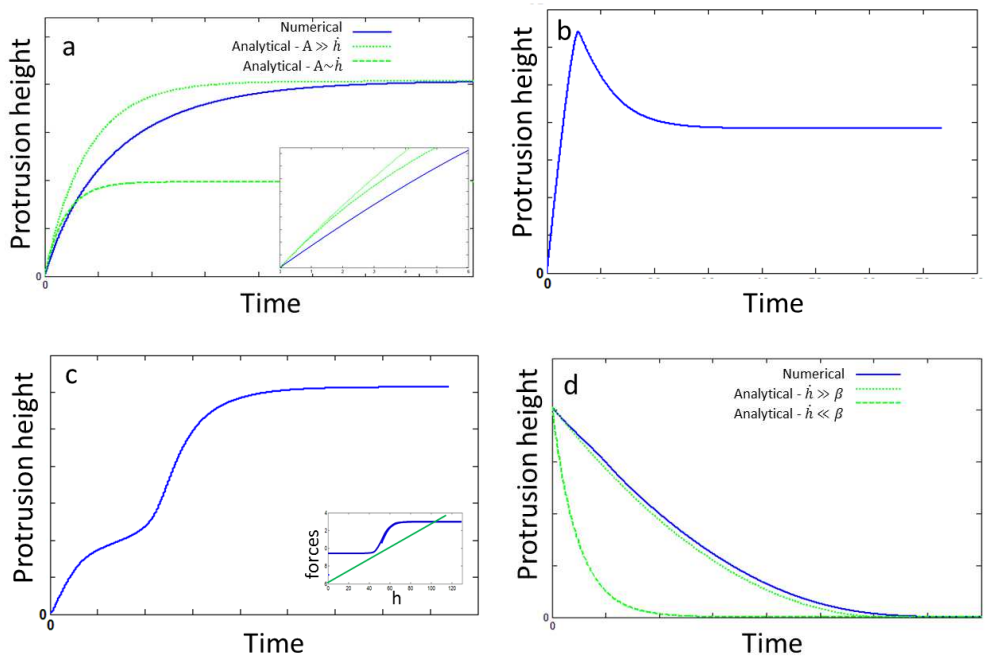

FIG. S2: The height dynamics of a cylindrical protrusion. a) A constant rate of polymerization and a monotonic restoring force with no initial tail (numerical solution in blue, analytical solutions in green: solid line case 1, dashed line case 2 in Table I). In the inset we highlight the initial growth stage showing that the real slope in smaller than A. b) Calculation with an initial long tail giving initial slope of $\dot{h} = A$ and an overshoot in the height above the steady-state value. c) The growth dynamics for the protrusive and restoring forces as shown in the inset (blue and green respectively). d) Retraction dynamics of the protrusion following the termination of the polymerization (numerical solution in blue and analytical solutions in green: solid line case 3 and dashed line case 4 of Table I).

This gives rise to a discontinuity in the steady-state height as a function of both the protrusion tip's radius R_{tip} and the cell's viscosity γ_c, as shown in Fig.S7.

ANALYSIS OF THE STEADY-STATE TIP-COMPLEX RADIUS

The concentration of free CL at the rim of the tip-complex (Eqs.14,18) as a function of the rim's radius ($\rho_f(R_{tip})$) is plotted in Fig.S8 for a range of protrusion heights. In the case where the protrusion is short enough ($h < z_1, |z_2|$) CL can diffuse outside ($J_{out}(0) \neq 0$) and $\rho_f(R_{tip} \to 0)$ is finite. For long protrusions $J_{out}(0) = 0$ and therefore $\rho_f(R_{tip} \to 0)$ can be very large and mathematically it diverges. An immediate conclusion from this behavior is that while it is possible to maintain a long protrusion at any radius, for short protrusion this is not always true and depends on the rates and concentrations of the nucleators and inhibitors. By controlling these parameters the cell can allow only protrusions above certain critical height to survive.

In all cases $\rho_f(R_{tip})$ decays over a length-scale of $\sqrt{D_{tip}/k_{tip}}$ (Fig.S8), and for $R_{tip} \gg \sqrt{D_{tip}/k_{tip}}$, $\rho_f(R_{tip})$ can be considered a constant. This means that for radii that are larger than this value the radius is very sensitive to fluctuations in the concentrations of CL, inhibitors and nucleators. i.e. small fluctuations in those parameters will result in huge changes in R_{tip}, in contrast to observations. We therefore conclude that in biological system one should expect $R_{tip} \ll \sqrt{D_{tip}/k_{tip}}$.

In Fig.S9 we plot the concentration of free CL+myosin complexes (Eqs.16,17), along the length of the protrusion, and at the protrusion tip. Due to the active transport towards the tip, the CL are highly localized at the tip, and their diffusive outflux is significant only when the protrusion height is small.

Analytical approximation for the steady-state radius

In the limit of short ($h \ll z_{1,2}$) and thin ($R_{tip} \ll \sqrt{D_{tip}/k_{tip}}$) protrusions, we can approximate $\rho_f(R_{tip})$ (Eqs.14,18) as

$$\rho_f(R_{tip}) = u_f(h) \simeq u_f(0) + \frac{u_f(0)(2k^u_{on}v_m - k_{tip}k^u_{off}R_{tip})}{2D_u k^u_{off}}h. \tag{S17}$$

Using this approximation in Eq.(21) we get the steady-state relation between the height and the tip radius

$$h_R \simeq \frac{2D_u k^u_{off}[\phi - u_f(0)]}{u_f(0)(2k^u_{on}v_m - k_{tip}k^u_{off}R_{tip})} \tag{S18}$$

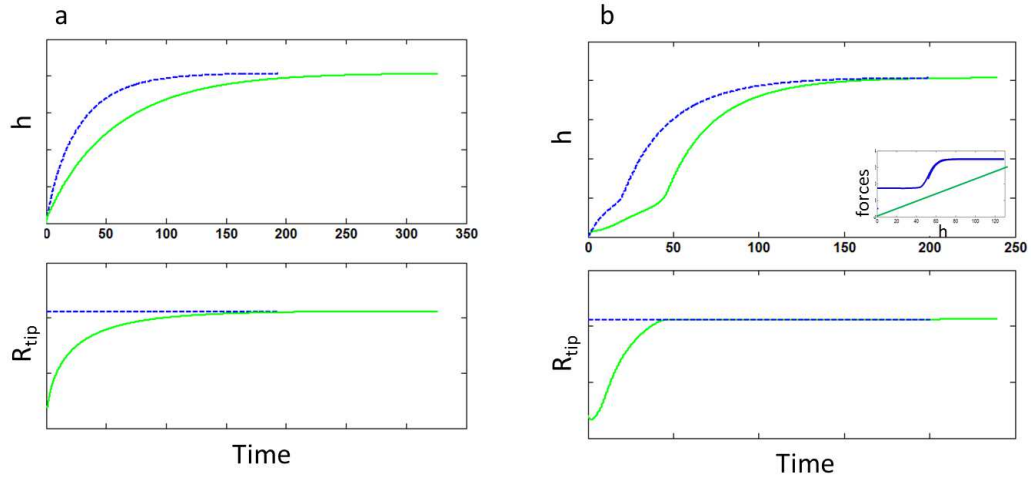

FIG. S3: The dynamics of both the protrusion radius and height as arise from the combination of the force model and the dynamic width regulation model. a) Constant polymerization rate. Dashed blue lines corresponds to the case of a constant radius as in Fig.S2 while solid green lines shows growing radius when $O(\tau_h) = O(\tau_R)$. b) Same as in (a) for height dependent polymerization rate, with the resulting protrusive and restoring forces as shown in the inset (blue and green respectively)..

where $\phi = \eta_{nuc}/k_{on}^{nuc}c_{nuc}$. This relation is plotted in Fig.S10 and is compared to the numerical solution of $R_{tip}(h)$. From (Eq.S18) we find that for short protrusions ($h < z_1, |z_2|$) the maximal radius is given by: $R_{max} = 2k_{on}^{u}v_m/k_{tip}k_{off}^{u}$. The critical height below which there are no solutions of finite radius is given by:

$$h_{min} = \frac{D_u k_{off}^u [\phi - u_f(0)]}{u_f(0) k_{on}^u v_m} \tag{S19}$$

Note that this is independent of k_{tip} and therefore independent of the actin polymerization rate (Eq.14). The increase of the height with the radius above the minimal value is linear, with a slope given by

$$\left.\frac{dh}{dR}\right|_{R=0} = \frac{D_u k_{tip} (k_{off}^u)^2 (\phi - u_f(0))}{2u_f(0)(k_{on}^u)^2 v_m^2} \tag{S20}$$

which increases with the polymerization rate (through k_{tip}, Eq.14). For $h \gg z_1, |z_2|$ the maximal radius is given by approximating (Eq.21) using Eq.(19):

$$R_{max} = \frac{2D_{tip}k_{off}^u \phi}{u_0 k_{on}^u v_m} \left(1 - \sqrt{1 - \frac{2u_0^2 k_{on}^u v_m^2}{\phi^2 (k_{off}^u)^2 D_{tip} k_{tip}}}\right). \tag{S21}$$

The condition for a finite solution is: $2u_0^2 k_{on}^u v_m^2 < \phi^2 (k_{off}^u)^2 D_{tip} k_{tip}$. We should note that comparison between the numeric solution and the analytical approximation for different parameter values reveals that the approximations give rather poor results for the values of h_{min}, $dh_R/dR_{R=0}$ and $R_{max}(h < z_1, |z_2|)$, but do capture correctly the dependencies of h_{min}, $dh_R/dR_{R=0}$ on the polymerization rate. Additionally the computed R_{max} (for $h \gg z_1, |z_2|$) proves to be a very good approximation of its exact value (Fig.S10).

ALTERNATIVE SHAPE MODEL BASED ON MEMBRANE-ACTIN ADHESION

Protrusion height

We demonstrate here another route to formation of protrusions with well defined height, that does not involve the protrusive force of actin polymerization, in contrast to the model explored in the main text. In order to envelope a cylindrical actin bundle by the plasma membrane of the cell, a binding between the membrane and the actin needs to exist in order to counterbalance the bending and stretching energy of the membrane deformation. Since the actin filaments that compose the bundle are continuously treadmilling, due to actin polymerization at their barbed ends (at the protrusion tip) and depolymerization at their pointed ends (at the protrusion base or inside the cytoskeleton bellow the protrusion), any membrane-actin binding protein will get washed out of the protrusion after some time. A binding protein that can diffuse in the membrane when not bound to actin will have a steady-state concentration

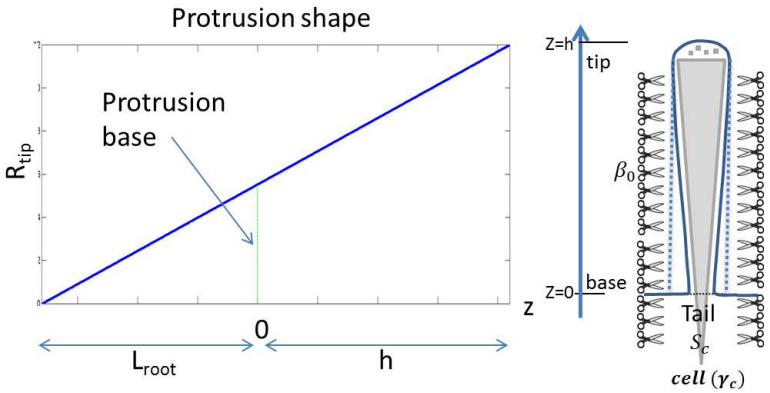

FIG. S4: When the severing is uniform along the entire protrusion the result is an actin bundle with a conical shape, with a slope of A/β. The rootlet length is denoted by L_{root}.

profile that is exponentially decaying from the protrusion base towards its tip [1]. A mechanism of activation of the binding proteins only at the protrusion tip [4] can induce an opposite gradient, having maximal membrane-actin binding at the protrusion tip and decaying towards the base.

Let us write the balance of forces that maintain the steady-state height of a single cylindrical protrusion with radius R in this case, where we ignore the role of actin treadmilling in providing any force. The constant restoring force due to the membrane deformation is given by

$$F_{mem} = 2\pi \left(\kappa \frac{1}{R} + \sigma R \right) \tag{S22}$$

The protrusive force due to membrane-actin binding is given by the derivative of the adhesion energy

$$\begin{aligned} E_{bind} &= -2\pi R \varepsilon_b \int_0^h \rho(z) dz \\ F_{bind} &= -\frac{\partial E_{bind}}{\partial z} = 2\pi R \varepsilon_b \rho(0) \end{aligned} \tag{S23}$$

where ε_b is the average binding energy per unit area (taking into account the relative binding probability of each motor: $k_{off}/(k_{on}+k_{off})$) and $\rho(z)$ is the local density of binding proteins along the protrusion. Eq.S23 simply states the additional energy gained per unit length of membrane annulus that is pulled from the surrounding and attached to the actin bundle, and is therefore dependent on the concentration of binding proteins at the protrusion base $\rho(0)$.

Passive actin-membrane adhesion molecules diffusing from the base

Due to the treadmilling the binding proteins have in general the following distribution [1]

$$\rho(z) = \rho_0 e^{(-z v_a k_{on}/D k_{off})} \tag{S24}$$

where v_a is the treadmilling velocity, D is the diffusion coefficient of the binding protein when not bound to actin, and k_{on}, k_{off} are the on/off rates for the binding/unbinding to actin.

In this case, since the concentration of binding proteins at the base is constant, $\rho(0) = \rho_0$, we have a constant protrusive force due to the binding proteins. If this constant force is larger than the constant restoring force from the membrane (Eq.S22), the protrusion can grow. However, above a certain height the binding density along the bundle will be too low, and the membrane could decrease its elastic energy by detaching from the actin bundle (see illustration in Fig.S11a).

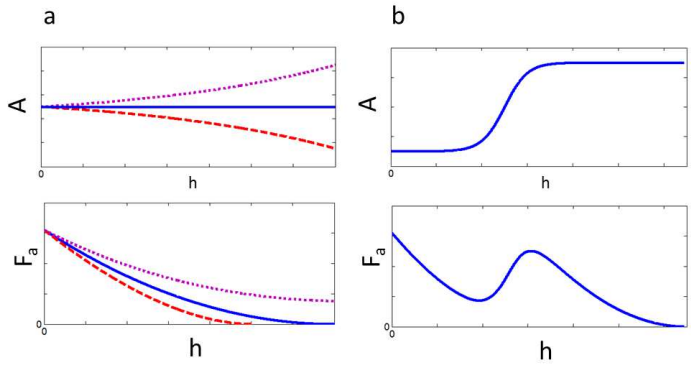

FIG. S5: The protrusive force due to actin (F_a) of a conical protrusion as a function of the height, for different height-dependent polymerization rate ($A(h)$). If the polymerization rate does not increase with h fast enough (condition in Eq.), the rootlet length and therefore the rootlet surface area decreases as the protrusion height increases. The protrusive force will therefore decrease with the decrease of the rootlet (a). If on the other hand the polymerization rate increases strongly enough with height then it compensate for the decrease in the rootlet surface area, resulting in an increase of $F_a(h)$ (b).

Passive actin-membrane adhesion molecules activated at the tip

Recently [4] a mechanism of activating passive actin-membrane adhesion at the protrusion tip was described. In this case the concentration of activated binding proteins decays from the tip towards the base, as the binding proteins are advected by the treadmilling actin and are de-activated at a constant rate α. The distribution becomes (assuming that the rate of production of activated proteins at the tip is constant)

$$\rho(z) = \rho_0 e^{-(h-z)/(v_a/\alpha)} \tag{S25}$$

as illustrated in Fig.S11b.

In the tension dominated regime, equating the restoring force of the membrane (Eq.S22) to the energy of the binding at the base of the protrusion (i.e. location at which the binding becomes too weak to hold the membrane on the actin core), gives the steady-state height

$$h_{ss} = \frac{v_a}{\alpha} Log\left[\frac{\rho_0 \varepsilon_b}{\sigma}\right] \tag{S26}$$

In the curvature-dominated regime the result becomes

$$h_{ss} = \frac{v_a}{\alpha} Log\left[\frac{\rho_0 \varepsilon_b R^2}{\kappa}\right] \tag{S27}$$

This result is interesting:

- The steady-state height is independent of the radius.
- Larger polymerization rate v_a increases the height, while tension σ and ERM-de-activation rate α decrease it.

Protrusion radius

So far the radius of the protrusion R was treated as another free parameter. We now demonstrate that the binding of the membrane to the actin bundle can also select a unique radius. Let us consider a finite surface area of the cell with a constant total number of cortical actin filaments N_T. This situation may be best realized for the brush-border microvilli, which form a uniform and dense array on the cell surface. In this case the number of protrusions is given

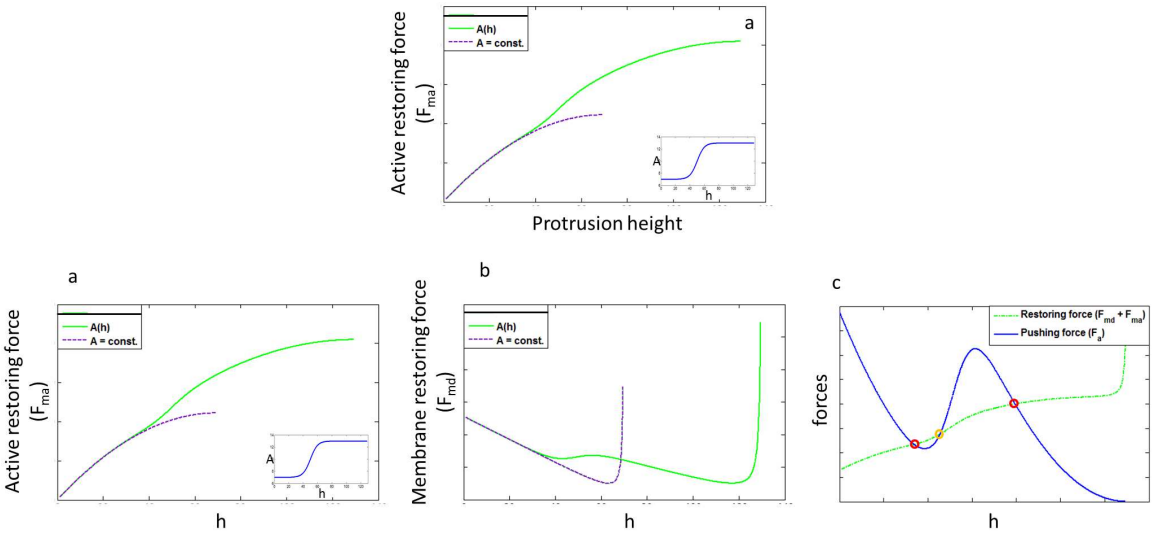

FIG. S6: The restoring force due to membrane-bound myosins (a) and due to the membrane deformation (b). The dashed purple line is for a constant polymerization rate and the solid green line for a polymerization rate that increases with the height $A(h)$ (as shown in the inset). (c) The pushing force (solid blue line) and the sum of all restoring forces (dashed green line). Red circles denote the stable steady-state solutions and the yellow circle the unstable solution.

by: $N_p = N_T a^2/R^2$, where a is the radius of an individual actin filament in the bundle (including the additional width due to adsorbed crosslinkers).

The total binding energy of the actin-membrane system is now (for simplicity consider a uniform distribution of motors along the protrusion: $\rho(z) = \rho_0$)

$$E_{bind} = -2\pi R \varepsilon_b \rho_0 h N_T \frac{a^2}{R^2} \tag{S28}$$

where the negative sign denotes that this is a binding energy. The membrane deformation energy is

$$E_{mem} = 2\pi \left(\kappa \frac{1}{R} + \sigma R \right) h N_T \frac{a^2}{R^2} \tag{S29}$$

Combining these expressions we find the equilibrium radius by taking the derivative to vanish

$$E_{tot} = E_{bind} + E_{mem} = 2\pi h N_T a^2 \left(\frac{\kappa}{R^3} + \frac{\sigma - \varepsilon_b \rho_0}{R} \right) \tag{S30}$$

$$\frac{\partial E_{tot}}{\partial R} = 0, \Rightarrow, R = \sqrt{\frac{3\kappa}{\varepsilon_b \rho_0 - \sigma}} \tag{S31}$$

In the limit that the binding is weak, such that $\varepsilon_b \rho_0/\sigma \to 1$, the width of the protrusion increase and a single protrusion contains all the actin bundles. As the binding strength increases the radius decreases. The cell could control the radius of the protrusions by modifying the density of motors and their affinity to actin.

Such a model would predict that increasing the binding of myosin-I to actin, or its overall concentration, would result in thinner protrusions.

* Corresponding author: nir.gov@weizmann.ac.il

[1] M. Naoz, U. Manor, H. Sakaguchi, B. Kachar, and N.S. Gov. Protein localization by actin treadmilling and molecular motors regulates stereocilia shape and treadmilling rate. *Biophysical journal*, 95(12):5706–5718, 2008.

[2] A.K. Rzadzinska, M.E. Schneider, C. Davies, G.P. Riordan, and B. Kachar. An actin molecular treadmill and myosins maintain stereocilia functional architecture and self-renewal. *The Journal of cell biology*, 164(6):887–897, 2004.

[3] T.M. Svitkina, E.A. Bulanova, O.Y. Chaga, D.M. Vignjevic, S. Kojima, J.M. Vasiliev, and G.G. Borisy. Mechanism of filopodia initiation by reorganization of a dendritic network. *The Journal of cell biology*, 160(3):409–421, 2003.

[4] A. Bretscher Viswanatha, R. and D. Garbett. Dynamics of ezrin and ebp50 in regulating microvilli on the apical aspect of epithelial cells. *Biochemical Society transactions*, 42(1):189–194, 2014.

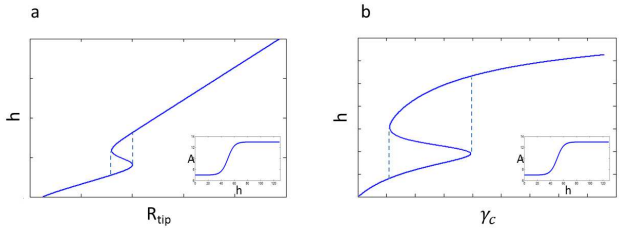

FIG. S7: The steady-state height of the protrusion as a function of the tip radius R_{tip} (a) and the cytoplasm viscosity γ_c (b). In both cases there is a region between the dashed lines in which there are two branches of stable solutions.

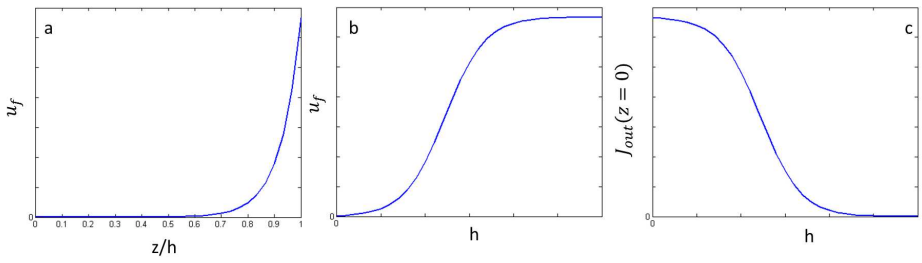

FIG. S9: Calculated steady-state concentration profile of the myosin+CL that are not bound to the actin bundle (u_f, Eqs.16,17) along the protrusion length (a), and as a function of the protrusion height (b) showing that the CL are concentrated close to the tip and that their concentration reaches saturation as a function of the height (due to the incorporation at the tip). (c) The diffusive outflux of CL at the base ($J_{out}(z=0)$). For long protrusions the outflux decreases to zero and the only way for the CL to exit the protrusion is by incorporation to the bundle at the tip.

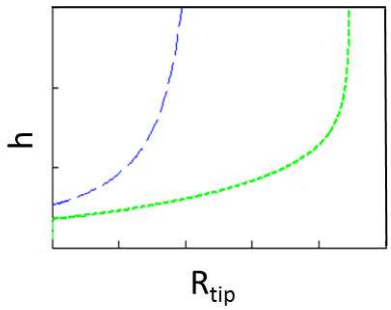

FIG. S10: A comparison between the full numerical solution for the steady-state width of the tip complex $R_{tip}(h)$ (green line, Eq.21) and the simplified analytic solution given in Eq.(S18) (blue line), for a constant polymerization rate.

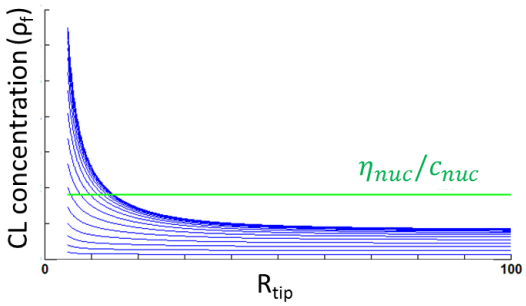

FIG. S8: The steady-state concentration of free CL at the rim of the tip complex as a function of the tip complex radius (Eqs.14,18). The different lines correspond to increasing protrusion heights (in ascending order). An increase in the height decreases J_{out} and therefore increases the CL concentration at the tip. The concentration decays over a length scale of $\sqrt{D_{tip}/k_{tip}}$, and reaches an asymptotic value for large radii. The CL concentration for which a steady-state radius exists is defined by the ratio η_{nuc}/c_{nuc} (Eq.21, horizontal green line). Note that for protrusion heights where the CL concentration is below the green line there are no solutions for any choice of radius.

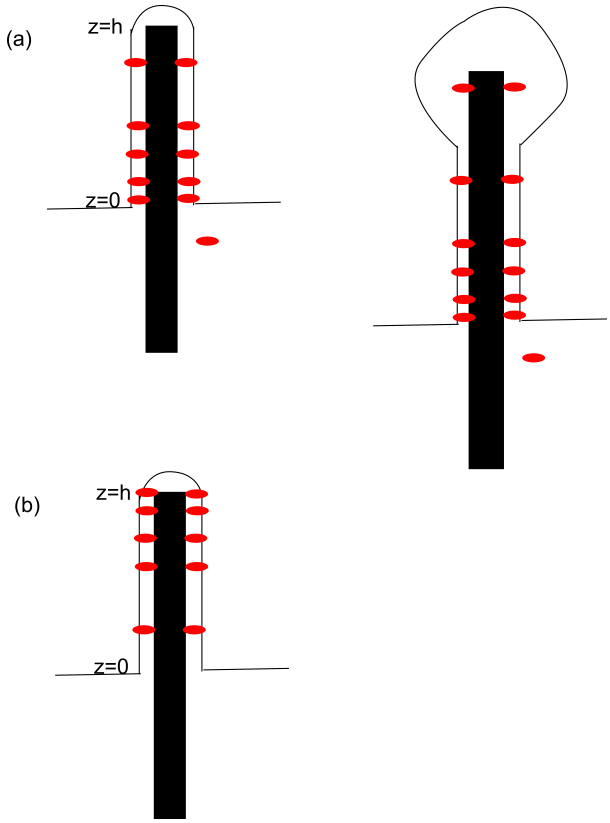

FIG. S11: Illustration of the growth of protrusions driven by membrane-actin binding. (a) If the binding proteins diffuse from the protrusion base, they are depleted from the tip region, which can then detach from the actin core. (b) For binding proteins that get activated at the tip, they are depleted from the protrusion base and this can select the steady-state protrusion height (Eqs.S26,S27).